Mass Transport Deposits Periodicity Related to Glacial Cycles and Marine-Lacustrine Transitions on a Ponded Basin of the Sea of Marmara (Turkey) Over the Last 500 ka

Céline Grall, Pierre Henry, Graham K. Westbrook, M Namik Çağatay, Yannick Thomas, Bruno Marsset, Daniel Borschneck, Hakan Saritaş, Günay Çifçi, Louis Géli

Mass Transport Deposits periodicity related to glacial cycles and marine-lacustrine transitions on a ponded basin of the Sea of Marmara (Turkey) over the last 500 ka

C. Grall[1,2*], P. Henry[1], G.K. Westbrook[2], M.N. Çağatay[3], Y. Thomas[2], B. Marsset[2], D. Borschneck[1], H. Saritas[4], G. Cifçi[4], L. Géli[2]

[1] CEREGE, CNRS, Aix Marseille University, Marseille, France

[2] IFREMER - French Research Institute for Exploration of the Sea, Marine Geosciences, Plouzané, France

[3] Istanbul Technical University, EMCOL and Department of Geological Engineering, Istanbul, Turkey

[4] Institute of Marine Sciences and Technology, Dokuz Eylul University, Izmir, Turkey

*grall@cerege.fr

Abstract

The Sea of Marmara (SoM) is affected by large earthquakes occurring on the North Anatolian Fault. Numerous submarine mass movements have occurred and the most recent turbidites in the basins of the SoM have been related to historical earthquakes. Within the SoM, the occurrence of submarine mass movements and their size appears modulated by eustatic changes that can be accompanied by transitions between a salty marine environment and a brackish lake environment. Detailed analysis, using a 3D high-resolution seismic dataset, of stratigraphy over the last 500 ka, within a ponded basin of the Western High, shows that intervals of draped sedimentary reflectors alternate with onlap sequences that followed episodes of rapid sea-level rise, with a periodicity of approximately 100,000 years (corresponding to glacial cycles). Mass Transport Deposits (MTDs) occur within the onlapping sequences. Detail analysis of the youngest large slide, which probably followed the lacustrine transition during Marine Isotopic Stage 4 is presented; and the possible triggering processes are discussed. The potential triggers of MTDs during this transition, in the context of the SoM are: (i) gas hydrate dissociation by pressure drop; (ii) changes in sediments supply and transport dynamics; (iii) variations in pressure and/or ionic strength in pores. The latter case appears the most suitable hypothesis, as salt diffuses out of the pores of the marine clay-rich sediment dominated by smectite at the beginning of low stand/lacustrine stages. The pore water freshening induces clay swelling, which can potentially drive sediment slope failure.

Keywords: High Resolution 3D seismic data, Mass Transport Deposits, lacustrine/marine transitions, Sea of Marmara

1. Introduction

A great variety of factors can cause and/or promote submarine mass movements, including earthquakes (Masson et al. 2006), environmental changes such as sea-level changes and associated variations in sediment supply (Rothwell et al. 1998), and gas hydrate dissociation (e.g. Maslin et al. 2004). The Sea of Marmara (SoM) is an active seismotectonic setting, located along the western part of the North Anatolian major continental transform fault (Wong et al. 1995; Le Pichon et al. 2001). Submarine gas hydrates occur in the sediment at fluid emission sites (Bourry et al. 2009). It is likely that hydrates were more widely distributed in the past and were dissociated massively during the deglaciation (Menot and Bard, 2010). The SoM has also been subjected to a history of connections and disconnections with Black and Aegean Seas via the Bosphorous and the Çannakale Straits respectively (Figure 1A, e.g. Cagatay et al. 2009). These oscillations are related to global eustatic changes, and induce transitions between lacustrine and marine conditions. In such an environment, submarine mass-movements are very common, and 75% of the sedimentation in basins is composed of gravity-induced deposits (e.g. Beck et al. 2007) and many of which were triggered by earthquakes (McHugh et al. 2006). Mass-wasting occurrence and size increased during the end of the glaciation period which may be attributed to thermal destabilization of gas hydrate or variations in sediment supply (Zitter et al. 2012).

During the last glacial period, the SoM was a mildly brackish lake (e.g. Londeix et al. 2009), as the global sea-level dropped below the level of the Çannakale sill (e.g. Çağatay et al. 2009) at the beginning of Marine Isotopic Stage 4 at ~70 ka (thereafter MIS-4). Sedimentation rates were at least two times higher during these glacial times than during modern marine environment (Cagatay et al. 2003; Vidal et al. 2010). Pore fluid composition profiles indicate diffusion of salts, between the lacustrine sediments and the seawater above, affecting a layer of 12-40 m thickness below the seafloor, that does not strongly depending on the sedimentation rates in the area considered (Zitter et al. 2008; Çağatay et al. 2004).

Little is known about older paleo-environmental changes induced by sea-level variations. Considering global sea-level variations (e.g. Lisieck and Raymo, 2005), marine to lacustrine transitions may not have occurred during all the glacial 100,000-year cycles, as the timing of connection and disconnection depends not only on global sea-level but also on the depth of the Çannakale sill, which probably varied with time (e.g. Çağatay et al. 2009; Badertscher et al. 2011).

In this paper, the relationship between mass wasting and sea-level changes over the last 400-500 ka is evaluated using high resolution seismic records. The Mass-

Transport Deposits (MTDs) related to sea-level oscillations and marine/lacustrine transitions are here characterized, and the possible MTDs trigger processes discussed.

2. Main observations and interpretations

2.1. Overview of stratigraphic sequences and Mass-Transport Deposits position

The 3D seismic survey covers an area of 33 km^2 on the western part of the Western High, along the main strike-slip fault branch of the Main Marmara Fault (MMF, Le Pichon et al. 2001, Figure 1B). We focus here on the Eastern Fault-Zone Basin, an asymmetric basin bounded on its southern side by the MMF (Figure 1B). The seismic imaging (migration, bin size 6 m, Thomas et al. 2012) has a maximum subseabed seismic penetration of about 600 m in this basin. H0, the shallowest seismic horizon (Figure 2) encountered over most of the 3D HR survey, is at around 15 m depth on core MD01-2430 location, at the same depth as an ash layer(Lericolais and Henry, 2004) Mean sedimentation rates over this time-scale have been derived from the H0 mapping. The sedimentation rates range between 0.3 and 1.1 mm/a, in the Eastern Fault-Zone Basin. Considering the seismic penetration and the sedimentation rates, the dataset gives access to the history of sedimentation over a time scale of about 500 000 years.

Sedimentary sections consist of the repetition of four sequences, each sequence has between 0 and around 80 meters of thickness and contains two seismic units (Figure 2A and B) : (1) Draped units with moderate lateral variations of thickness, either acoustically transparent or bearing laterally continuous internal sub-parallel reflectors (2) Basin filling units displaying strong lateral variations of thicknesses and laterally correlative with either condensed sections (Figure 2B) or hiatuses on the slopes and topographic highs. Sedimentary bodies that contain irregular lenses and chaotic reflections are observed at the base and/or within the filling sequences (Figure 2A and B), and are interpreted MTDs (e.g. Alves et al. 2010).

Three remarkable MTDs thus occur within the basin filling units (Figure 2A). Prominent reflective horizons (H1, H4 and H6; Figure 2B) which present significant disruption, mark the base of the MTDs. The top horizons of the MTDs ($H1^0$, H3 and H5, Figure 2B), pinch out against a continuous basal horizons and display small-scale topography. Horizon H5 displays erosive channel geometry that may have developed concurrently with the deposition of the basin filling unit (Figure 2A and B). Erosion affects the underlying MTDs and therefore must at least in part post-date the MTDs events. Horizon H3 is relatively smooth but small erosive channels affect H4 where H3 is absent, suggesting the MTD strata between H3 and H4 is correlative with an erosion surface (Figure 2A and B).

The high-resolution age model from ^{14}C calibrated ages obtained from core MD01-2430 (Figure 1B) indicates a sharp reduction of sedimentation rate from 0.6 to 0.2 mm/a following the reconnection at 14.7 ka (Vidal et al. 2010). In the Holocene, sedimentation rates subsequently increased back to 0.4 mm/a, although still not reaching the glacial sedimentation rate again (Vidal et al. 2010). We surmise this has been the case during previous glacial cycles, at least in cases when the SoM had been disconnected during a global sea-level low-stand, and possibly during all episodes of rapid seal-level rise. In this case, the repetition of filling unit/draped section corresponds to the sea level low and high stands oscillation at 100 ka timescale. In particular, the onlap sequence on H1' (Figure 2C and D), first low-stand/filling units below the seafloor, probably results from a decrease of sedimentation rate during the marine high stand at MIS-5 (~130 ka). The MTDs lying on H1 thus occurred during the sea level fall at MIS-4 (~70 ka).

Variations of clay composition could explain differences of slope instabilities frequency between marine and lacustrine rich-clay sediments. Powder of clay fraction of 38 samples (of both marine and lacustrine muds) has been characterized by X-ray diffraction. The relative amount of smectite, illite, kaolinite and chlorite were determined by comparing the major XRD reflection peaks surfaces obtained on untreated, ethylene-glycolated, hydrazine monohydrate and heated smear slides. Lacustrine and marine clay compositions do not display significant differences. The clays fraction is dominated by swelling clay as the clay fraction is composed of, on average, 75% smectite, 13% illite, and around 5-7% kaolinite and chlorite.

2.2 Characterization of MTDs on H1

The MTDs above H1 form a thick unstratified lens with a rough upper surface. Within this lens, we observed locally some highly reflective patches interpreted as stratigraphic reflectors within coherent blocks floating in a matrix of flowed mud that has lost coherence, at least at the scale of the HR data (Figure 3D). The top of the MTDs is a highly reflective and rough reflector of reverse polarity to that of the seafloor, suggesting that the deposit has probably a higher content of fluid than the upper sediments. The top of the MTD is undulated, and we observed small-scale ridges of higher reflectivity (in absolute value) with a NE-SW strike (Figure 3B and C). The geometry of the structures suggests the mud flow occurred perpendicular to the western ridges (Figure 3A) along a NW-SE sliding direction. The MTD covers an area of about 0.47 km^2 and has a total volume of 5.5 hm^3. Along the NW edge of the basin, the MTD thickness is around 7-8 m. It increases toward the southeast, reaching a maximum thickness of 23 m in the central part of the basin (Figure 3C). H1 displays variable reflectivity below the MTDs. On the whole western edge of the MTDs but also its northeastern edge, H1 has negative polarity and high reflectivity (Figure 3A). Below the central part of the MTDs, H1 appears composite with several sub-reflectors resulting in a concentric reflectivity pattern (Figure 3A). On the slope west of the MTD, H1 is absent, or displays low reflectivity, over a 0.28 km^2 area (labeled eroded area in Figure 3A). This area corresponds to a place where

158 H1 but also others horizons above have been eroded and thus appears as the proba-
159 ble main source of the material forming the slide masses. The thickness of sediment
160 removed during the event is estimated to 11±5 m comparing the thickness of sedi-
161 ment on either side of the slide with the thickness of sediment in the scar (Figure
162 3D, section 1-1'). It also seems that most of the sediment deposited between H1 and
163 H0 has been removed. The volume of sediment removed is thus $3\pm1.4 \times 10^6$ m^3,
164 which represents only about 1/2 to 1/3 of the MTD volume. This paradox may be
165 resolved if sediments deposited above H1 in the basin have been displaced and in
166 part incorporated into the MTD. The eastern edge of the MTD is not sharp (Figure
167 3D, section 2-2') but appears as a gradational transition between disturbed sedi-
168 ments and an undisturbed layer of about 7-8 m thickness. Also, the base of the MTD
169 is not erosive in the deepest parts of the basin but appears to follow closely H1,
170 which may represent the basal sliding surface or layer immediately beneath it. In
171 fact the volume and geometry of the MTD may be accounted for, if a 7.4 m average
172 thickness layer of sediment covering both the area of sediment removal and the area
173 now covered by the MTD was redistributed by the sliding event to the deeper part
174 of the basin. This can suggest liquefaction occurred as the slide progressed, a com-
175 mon feature in slides and slumps, which can evolve into debris flow deposits
176 (Mulder and Cochonat, 1996).

177 3. Discussions about possible triggering processes and
178 conclusions:

179 During the last glacial cycle, the draped sequence in the basin corresponds to
180 low-stand lacustrine deposits with a relatively high sedimentation rate. Parts of the
181 underlying deposits, presumably marine sediments from the last interglacial (MIS-
182 5), have been redistributed by gravitationally driven mass transport, resulting in lat-
183 eral variations in sediment thickness. Sediment remobilization likely occurred after
184 sea-level dropped at MIS-4. This pattern of alternating draping sedimentation and
185 sediment redistribution is found to repeat cyclically in the stratigraphic record. This
186 suggests that comparable sequences of events occurred during earlier glacial cycles.
187 This is also supported by the thickness of these sequences, which would correspond
188 to about 100,000 years of sedimentation extrapolating the mean sedimentation rates
189 measured over the last ~29 ka.
190 Sediment fluxes into the deep basins of the Sea of Marmara from continental
191 shelves and slopes are higher during low stand than during high stand, and slope
192 instabilities clustered at the end of the glaciation (Zitter et al. 2012). However, the
193 Western High is relatively isolated from this influence, as canyons originating from
194 the shelf edges bypass the Western High and supply sediments to the deep Central
195 and Tekirdag basins (Figure 1A). Nevertheless, we still observe cyclic local redis-

196 tribution of sediments between slopes and ponded basinsbut probably with a differ-
197 ent timing as the MTD in this study is inferred to correlate with the beginning of a
198 low stand.
199 At the beginning of MIS-4 (~70 ka), sea-level fell from -25 m to -85 m below
200 the modern sea level resulting in the disconnection of the Sea of Marmara (Çağatay
201 et al. 2009). This also induced a pressure drop of 0.6 MPa and thus possible disso-
202 ciation of gas hydrate (Liu & Flemings, 2009). Nonetheless, a temperature decrease
203 of 1°C at the seafloor of the Western High associated to this pressure drop should
204 be sufficient to keep hydrates in their stability field (e.g, Henry et al. 1999). It is
205 thus unlikely that widespread gas hydrate dissociation occurred at this time. On the
206 other hand, pore fluid freshening by salt diffusion must have occurred. Since the
207 post-glacial reconnection, water column salinization (that has been progressive over
208 2000 years, Vidal et al. 2010) lead to the diffusion of salts downward into the pore
209 fluids of the lacustrine sediments (Zitter et al. 2008) and the reverse process had
210 occurred during the last glaciation after the disconnection. The diffusion length be-
211 ing proportional to the square root of time, the salt diffusion gradient below the
212 seafloor affects a sediment layer of thickness 10 to 100 m for times ranging from
213 1000 to 100.000 years. A layer of 11±5 m of marine sediments has been remobi-
214 lized, which appears consistent with the thickness of leached sediments after only a
215 few thousand years. As the clay-fraction is dominated by smectite, clay swelling
216 induced by osmotic stress during the desalinization of the pore water is expected
217 (Charpentier and Bourrié, 1997), reducing the cohesion of sediment and promoting
218 submarine slope failures (Masson et al. 2006). Consequently, systematic destabili-
219 zation of marine sediments on slopes at the beginning of lacustrine periods should
220 occur.
221 We remarked that the cyclic occurrence of MTDs observed in a ponded basin of
222 the Western High in the SoM could correlate with glacial-interglacial sequences.
223 Despite that slope instabilities are presumably triggered by earthquakes, their size
224 and/or frequency appears to be modulated by glacio-eustatic oscillations and the
225 lacustrine/marine transitions associated to them. The swelling of clays in marine
226 sediments under low salinity brackish water can promote slope instability after ma-
227 rine to lacustrine transitions, and may be one factor contributing to long-term cy-
228 clicity of slope instability occurrence in the Sea of Marmara.
229

Figure captions

Figure 1 : A. Tectonic map of the Sea of Marmara region with the Main Marmara Fault (MMF, Le Pichon et al. 2001) and secondary fault system (Grall et al. 2012). The red box locates the 3D seismic survey data. B. Seafloor mapping from the 3D-seismic data, and the location of the Eastern Fault-Zone basin (annotated EFZ-basin). Locations of the seismic lines present on Figure 2, MD01-2430 core, and sites where gas hydrates have been sampled are shown. The black box indicates the area shown in Figure 3A.

Figure 2 : A. Seismic section across the northern edge of the Eastern Fault-Zone Basin. MTDs are highlighted in yellow, and numbers 1, 2, 3 refer to the three most remarkable MTDs discussed in the text. B. Line drawing of the seismic section above. Horizon numbers mentioned increase from top to bottom. Stratigraphic sequences contain one basin filling unit (in grey) in which MTDs occurred (indicate by black stars), and one draped section (in white). The four main stratigraphic sequences in this characteristic seismic section have a thickness of around 65-75 ms twt, which represent around 50-63 m (P-wave velocity ranges between 1515 (above H1) and 1660 m/s (between H6 and H4), within the sediments, Thomas et al, 2012). C: Seismic section across the Eastern Fault-Zone Basin, showing details of the first stratigraphic sequence below the seafloor. D. Line drawing of the seismic section above. The filling unit contains a condensed section (H1'-H1) on which MTDs occurred (between H1 and $H1^0$). The condensed section extension corresponds to the basin depocentre (represented in Figure 3A) when the slides occurred. See Figure 1C for the location of the seismic lines.

Figure 3 : Mapping and characteristics of the first remarkable MTDs below the seafloor, which probably occurred after the sea-level fall at MIS-4 (~70 ka). A. Amplitude map of the basal surface of the MTDs (horizon H1). This map is located in Figure 1B. Eroded area and area of deposits (which is detailed in Figure 2B and C) correspond to the main scars of the slides and the zone of slide depositions. The depocentre is derived from the mapping of the condensed section below the MTDs (Figure 2C and D). B. Amplitude map of the top horizon of the MTDs. Amplitude anomalies alignment is indicated by white dash lines. C. Topography of the top horizon of the MTDs. The white dash lines and the black arrows indicate the orientation of small undulations and the flow lines respectively. D. Seismic sections along the scars of the slides (1-1') and across the MTDs (2-2').

Acknowledgements

The Marmara-DM cruise was supported by ESONET NoE, Network of Excellence, coordinated by IFREMER and co funded by EU as part of FP6 (2009).This work is also co-funded by CNRS. We would like to thank Cedric Amiel, for his participation to the XRD laboratory manipulation. We thank Cecilia McHugh and Lies Loncke for their constructive comments that improved this manuscript.

4. References:

Alves TM (2010), 3D Seismic examples of differential compaction in mass-transport deposits and their effect on post-failure strata, Marine Geology, 271: 212-224.

Badertscher S, Fleitmann D, Cheng H et al (2011), Pleistocene water intrusions from the Mediterranean and Caspian seas into the Black Sea, Nature Geosci, 4: 236-239.

Beck C, Mercier de Lepinay B, Schneider JL et al (2007), Late Quaternary co-seismic sedimentation in the Sea of Marmara's deep basins, Sedimentary Geology, 199: 65-89.

Bourry C, Chazallon B, Charlou JL et al (2009), Free gas and gas hydrates from the Sea of Marmara, Turkey: Chemical and structural characterization, Chemical Geology, 264: 197-206.

Cagatay MN, Ozcan M, Gungor E et al (2004), Pore-water and sediment geochemistry in the Marmara Sea (Turkey): early diagenesis and diffusive fluxes, Geochemistry-Exploration Environment Analysis, 4: 213-225.

Cagatay MN, Eris K, Ryan WBF et al (2009), Late Pleistocene-Holocene evolution of the northern shelf of the Sea of Marmara, Marine Geology, 265: 87-100.

Charpentier, S. Bourrié, G. (1997), Deformation of saturated clays under mechanical and osmotic stress and its relation with the arrangement of the clays, European Journal of Soil Science, 48: 49-57.

Grall C, Henry P, Tezcan D et al (2012), Heat flow in the Sea of Marmara Central Basin: Possible implications for the tectonic evolution of the North Anatolian fault, Geology, 40: 3-6.

Henry P, Thomas M, Ben Clennell, M (1999), Formation of natural gas hydrates in marine sediments 2. Thermodynamic calculations of stability conditions in porous sediments, J. Geophys. Res., 104 : 23005-23022.

Lericolais, G., Henry, P., 2004. Cruise report of Marmara VT / Marmacore 2. http://www.
cdf.u-3mrs.fr/~henry/marmara/marmaraVT.html2004.

Le Pichon X, Sengor AMC, Demribag E, et al (2001), The active Main Marmara Fault, Earth and Planetary Science Letters, 192: 595-616.

Lisiecki LE., Raymo ME (2005), A Pliocene-Pleistocene stack of 57 globally distributed benthic d18O records, Paleoceanography, 20: PA1003.

Londeix, L., Herreyre Y, Turon JL, et al (2009), Last Glacial to Holocene hydrology of the Marmara Sea inferred from a dinoflagellate cyst record, Review of Palaeobotany and Palynology, 158: 52-71.

Maslin M, Owen M, day S, et al (2004), Linking continental-slope failures and climate change: Testing the clathrate gun hypothesis, Geology, 32: 53-56.

Masson DG, Harbitz CB, Wynn RB, et al (2006), Submarine landslides: processes, triggers and hazard prediction, Philosophical Transactions of the Royal Society A: Mathematical, Physical and Engineering Sciences, 364 : 2009-2039.

McHugh CMG, Seeber L, Cormier MH et al (2006), Submarine earthquake geology along the North Anatolia Fault in the Marmara Sea, Turkey: A model for transform basin sedimentation, Earth and Planetary Science Letters, 248 : 661-684.

Menot, G., and E. Bard (2010), Geochemical evidence for a large methane release during the last deglaciation from Marmara Sea sediments, Geochimica Et Cosmochimica Acta, 74 : 1537-1550.

Mulder T, Cochonat P, Classification of offshore mass movements, Journal of Sedimentary Research, 66: 43-57.

Rothwell RG, Thomson J, Kahler G. (1998), Low-sea-level emplacement of a very large late Pleistocene "megaturbidite" in the Western Mediterranean Sea, Nature, 392 : 377-380.

Seeber L, Cormier MH, McHugh C, et al (2006), Rapid subsidence and sedimentation from oblique slip near a bend on the North Anatolian transform fault in the Marmara Sea, Turkey, Geology, 34 : 933-936.

Thomas Y; Marsset B; Westbrook GK.;et al (2012), Contribution of high-resolution 3D seismic near-seafloor imaging to reservoir-scale studies: application to the active North Anatolian Fault, Sea of Marmara, Near Surf. Geophys., 10 : 291-301.

Vidal, L., Menot G., Joly C. et al (2010), Hydrology in the Sea of Marmara during the last 23 ka: Implications for timing of Black Sea connections and sapropel deposition, Paleoceanography, 25: PA1205.

Wong, H. K., Ludmann T., Ulug, A. et al (1995), The Sea of Marmara - a Plate Boundary Sea in an Escape Tectonic Regime, Tectonophysics, 244 : 231-250.

Zitter TAC; Henry P; Aloisi G; et al (2008), Cold seeps along the main Marmara Fault in the Sea of Marmara (Turkey), Deep-Sea Research Part I-Oceanographic Research Papers, 55: 552-570.
Zitter T AC., Grall C; Henry, P et al (2012), Distribution, morphology and triggers of submarine mass wasting in the Sea of Marmara, Marine Geology, 329: 58-74.

5. Figures:

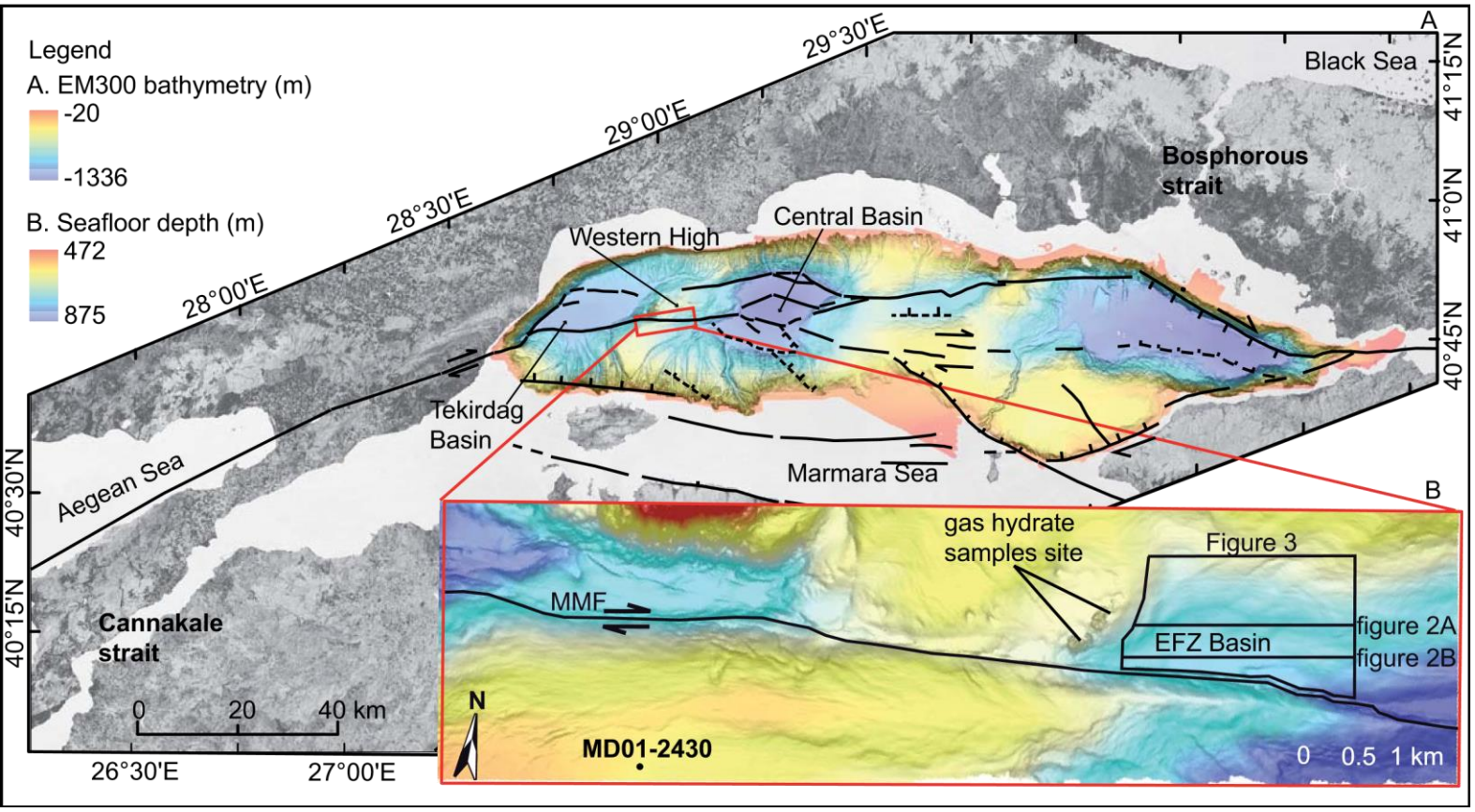

332

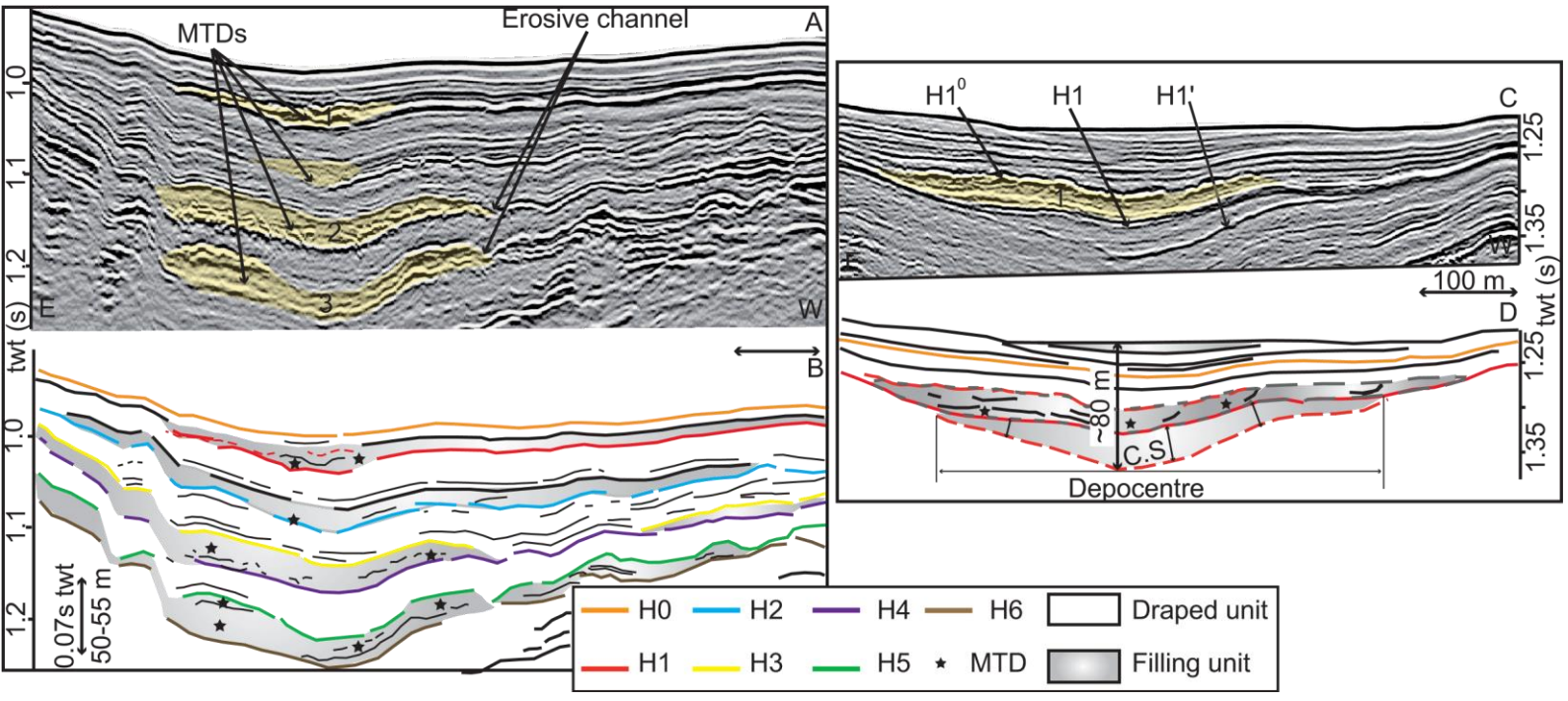
MTDs
Erosive channel
A
1
2
3
E
W
1,0
1,1
1,2
twt (s)
B
0.07s twt
50-55 m
H1⁰
H1
H1'
C
100 m
D
~80 m
C.S
Depocentre
1.25
1.35
H0
H2
H4
H6
Draped unit
H1
H3
H5
MTD
Filling unit

333
334

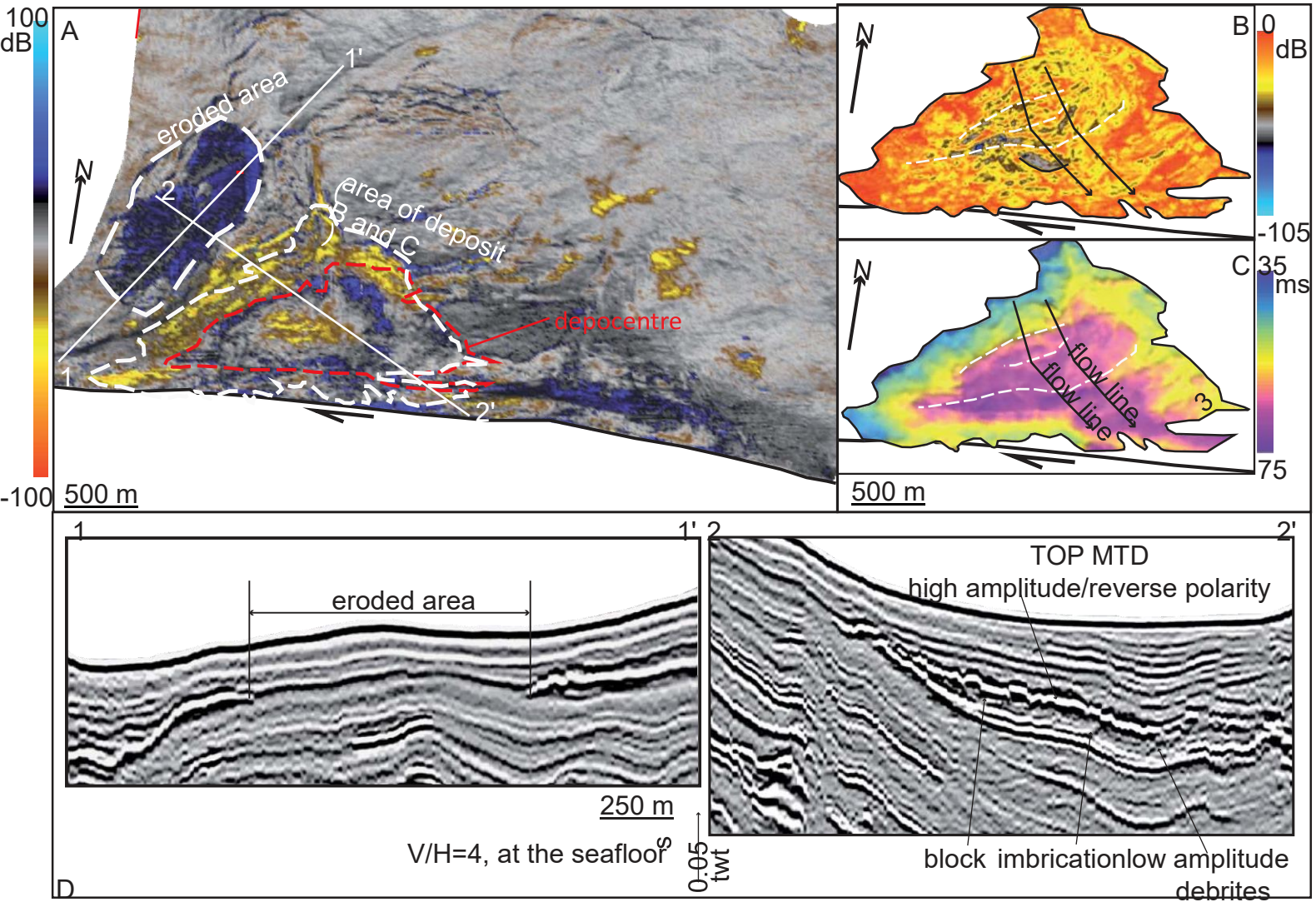
100
dB
-100
A
N
eroded area
1'
2
area of deposit
B and C
depocentre
1
2'
500 m
B
0
dB
-105
C
35
ms
75
flow line
flow line
3
500 m
1
1'
2
2'
eroded area
250 m
V/H=4, at the seafloor
0.05
s
twt
TOP MTD
high amplitude/reverse polarity
block
imbrication
low amplitude
debrites
D